arXiv:0806.4810v1 [cond-mat.mes-hall] 30 Jun 2008

Finite size effects of helical edge states in HgTe/CdTe quantum wells

Bin Zhou[1,2], Hai-Zhou Lu[1], Rui-Lin Chu[1], Shun-Qing Shen[1], and Qian Niu[3]

[1] *Department of Physics, and Center for Theoretical and Computational Physics, The University of Hong Kong, Pokfulam Road, Hong Kong, China*

[2] *Department of Physics, Hubei University, Wuhan 430062, China*

[3] *Department of Physics, The University of Texas at Austin, Austin, Texas 78712, USA*

(Dated: June 30, 2008)

The solutions for the helical edge states for an effective continuum model for the quantum spin Hall effect in HgTe/CdTe quantum wells are presented. For a sample of a large size, the solution gives the linear dispersion for the edge states. However, in a finite strip geometry, the edge states at two sides will couple with each other, which leads to a finite energy gap in the spectra. The gap decays in an exponential law of the width of sample. The magnetic field dependence of the edge states illustrates the difference of the edge states from those of a conventional quantum Hall strip of two-dimensional electron gas.

PACS numbers: 73.43.-f, 72.25.Dc, 85.75.-d

Recent discovery of quantum spin Hall (QSH) effect brings the Hall family a new member, an insulator with topological properties of electron bands distinct from the conventional ones [1]. Kane and Mele [2] proposed that newly synthesized graphene may exhibit a QSH effect. This novel state consists of the helical edge states whose dispersions locate inside the bulk insulating gap. They indicated that the Z_2 topological number distinguishes between the QSH and usual insulating phases. Benevig *et al* [3] realized that the HgTe/CdTe quantum well is a potential candidate for observing this effect based on the fact that the electron bands changes from the normal to an "inverted" type at a critical thickness of the quantum well, which was confirmed experimentally within one year.[4] Several other candidates were also proposed, such as GaAs with shear strain [5] and a multilayer Bi thin film[6]. Up to now, considerable efforts have been done to explore the properties of the QSH effect and topological insulators [7]. One of the striking properties is the crossing linear dispersions of the two edge states in which the electric currents with different spins flow in opposite directions. Very recently, it was reported that the massive Dirac particles exist in the bulk of $Bi_{0.9}Sb_{0.1}$, which is a hall mark of higher dimensional quantum spin Hall insulator.[8]

The theory of QSH effect in HgTe/CdTe was based on an effective 4-band model of the HgTe/CdTe quantum well that participates in the inversion crossing of electron and hole bands derived by Benervig, Hughes and Zhang [3]. Until present almost all works are based on numerical solutions of the model in a tight-binding method [2, 9, 10]. It was argued that the QSH insulator state has gapless and linear dispersions locating inside the bulk insulating gap. In the present Letter, we present the solution for the edge states of the 4-band model. In a finite strip geometry, linear dispersions for four edge states are reproduced for a sufficient large sample comparing with the space distribution scale of the edge states. However, when the size of sample is comparable with the size scale of the edge state, the edge states near the crossing point will couple with each other and open a finite energy gap. The gap decays in an exponential law with the size of the sample. This demonstrates that the edge states of QSH effect are quite different from the edge states of quantum Hall (QH) effect.

Here we start from the effective 4-band model for HgTe/CdTe quantum wells [3]

$$\mathcal{H}(k_x,k_y)=\begin{pmatrix} H(k) & 0 \\ 0 & H^*(-k)\end{pmatrix}, \tag{1}$$

where $H(k)=\epsilon_k\mathbf{I}_2+d^a(k)\sigma^a$, with $\mathbf{I}_2$ being a 2×2 unit matrix, σ_a the Pauli matrices, $\epsilon_k=C-D\left(k_x^2+k_y^2\right)$, $d^1=Ak_x$, $d^2=Ak_y$, and $d^3=\mathcal{M}(k)=M-B\left(k_x^2+k_y^2\right)$. A, B, C, D, and M are material specific parameters that are functions of the thickness of the quantum well. The model is derived from the Kane model near the Γ point in a heterojunction of HgTe/CdTe, and its validity is limited for small values of $k_{x,y}$. The most striking property of this system is that the mass or gap parameter M changes sign when the thickness d of the quantum well is varied through a critical thickness d_c (= 6.3 nm) associating with the transition of electronic band structure from a normal to an "inverted" type [11]. We will now solve this continuum model (1) in a finite strip geometry of the width L with the periodic boundary condition in the x direction and an open boundary condition in the y direction. In this case, k_x is a good quantum number but k_y is replaced by using the Peierls substitution $k_y=-i\partial/\partial y=-i\partial_y$. The Hamiltonian (1) is block-diagonal, and the upper $\hat{H}_\uparrow$ $(=H(k))$ and lower $\hat{H}_\downarrow$ $(=H^*(-k))$ blocks describe the states of spin-up and spin-down, respectively. The eigenvalue problem of the upper and lower blocks can

be solved separately, i.e., $\hat{H}_{\uparrow}\Psi_{\uparrow} = E\Psi_{\uparrow}$ and $\hat{H}_{\downarrow}\Psi_{\downarrow} = E\Psi_{\downarrow}$ with $\Psi_{\uparrow}(k_x, y) = e^{ik_x x}(\psi_1(k_x, y), \psi_2(k_x, y))^T$ and $\Psi_{\downarrow}(k_x, y) = e^{ik_x x}(\psi_3(k_x, y), \psi_4(k_x, y))^T$ where T means "transpose". Because the lower block of the Hamiltonian is the time reversal of the upper block of the Hamiltonian, the solution $\Psi_{\downarrow}(k_x, y) = \Theta\Psi_{\uparrow}(k_x, y)$, where $\Theta = -i\sigma_y K$ is a "time-reversal" operator and K stands for complex conjugation. Thus we can only focus on the solution for the upper block of this Hamiltonian.

The set of the eigenvalue equations for the upper block is expressed as

$$\left[M - B_+\left(k_x^2 - \partial_y^2\right)\right]\psi_1 + A\left(k_x - \partial_y\right)\psi_2 = E\psi_1, \quad (2)$$
$$A\left(k_x + \partial_y\right)\psi_1 - \left[M - B_-\left(k_x^2 - \partial_y^2\right)\right]\psi_2 = E\psi_2, \quad (3)$$

with $B_{\pm} = B \pm D$. From eqs. (2) and (3), using the trial function $\psi_{1,2} = e^{\lambda y}$, the characteristic equation gives four roots $\pm\lambda_1$ and $\pm\lambda_2$,

$$\lambda_{1,2}^2 = k_x^2 + F \pm \sqrt{F^2 - (M^2 - E^2)/B_+B_-}. \quad (4)$$

where $F = \frac{A^2 - 2(MB+ED)}{2B_+B_-}$. With the boundary conditions of $\Psi_{\uparrow}(k_x, y = \pm L/2) = 0$, we have an analytical expression for the wave function $\Psi_{\uparrow}$

$$\psi_1 = \tilde{c}_+ f_+(k_x, y) + \tilde{c}_- f_-(k_x, y), \quad (5)$$
$$\psi_2 = \tilde{d}_+ f_+(k_x, y) + \tilde{d}_- f_-(k_x, y), \quad (6)$$

with

$$f_+(k_x, y) = \frac{\cosh(\lambda_1 y)}{\cosh(\lambda_1 L/2)} - \frac{\cosh(\lambda_2 y)}{\cosh(\lambda_2 L/2)}, \quad (7)$$
$$f_-(k_x, y) = \frac{\sinh(\lambda_1 y)}{\sinh(\lambda_1 L/2)} - \frac{\sinh(\lambda_2 y)}{\sinh(\lambda_2 L/2)}. \quad (8)$$

The non-trivial solution for the coefficients $\tilde{c}_{\pm}$ and $\tilde{d}_{\pm}$ in the wave functions leads to a secular equation

$$\frac{\tanh\frac{\lambda_1 L}{2}}{\tanh\frac{\lambda_2 L}{2}} + \frac{\tanh\frac{\lambda_2 L}{2}}{\tanh\frac{\lambda_1 L}{2}} = \frac{\alpha^2\lambda_2^2 + \beta^2\lambda_1^2 - k_x^2(\alpha - \beta)^2}{\alpha\beta\lambda_1\lambda_2}, \quad (9)$$

where $\alpha(E) = E - M + B_+k_x^2 - B_+\lambda_1^2$, and $\beta(E) = E - M + B_+k_x^2 - B_+\lambda_2^2$. Eqs. (4) and (9) determine the energy spectra of the upper block $\hat{H}_{\uparrow}$.

Let us first consider the general properties of the solution for $\lambda_{1,2}$. In a large L limit, a purely imaginary $\lambda = ik_y$ is always the solutions of the equation, and gives two branches of spectra, $E_{\pm} = \epsilon_k \pm \sqrt{(M - Bk^2)^2 + A^2k^2}$. These are the bulk spectra and revised by the A-term slightly, and corresponding solutions span in the whole space. Except for these imaginary solutions, there also exist real solutions when

$$A^2/B_+B_- > \max\{2M/B, 4M/B\}. \quad (10)$$

In the large L limit, $\tanh(\lambda_{1,2}L/2) = 1$, and Eq. (9) gives

$$E_{\pm} = M - B_+\lambda_1\lambda_2 \pm B_+(\lambda_1 + \lambda_2)k_x - B_+k_x^2. \quad (11)$$

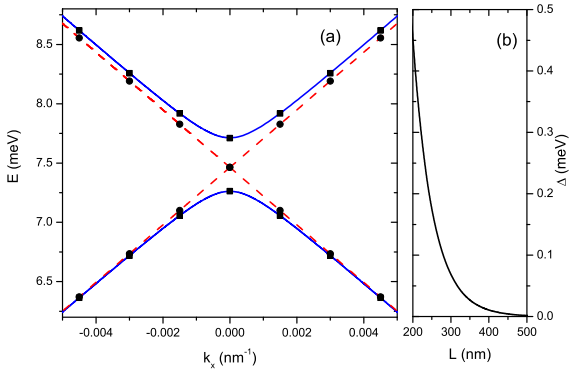

FIG. 1: (Color online) (a) Energy spectra of edge states for $L = 200$ nm (blue solid lines) and $L = 1000$ nm (red dashed lines) by solving eqs. (4) and (9) for the HgTe/CdTe quantum well thickness $d = 7.0$ nm. The parameters are given in the text. As a comparison, numerical results of tight binding approximation, which was used in Ref.[9] for the same parameters are also plotted as black squares for $L = 200$ nm and black dots for $L = 1000$ nm. (b) The width dependence of the energy gap Δ for a finite width strip of HgTe/CdTe quantum well of thickness $d = 7.0$ nm. Specifically, $\Delta(L = 200$ nm$) = 0.4509$ meV, $\Delta(500$ nm$) = 1.6 \times 10^{-3}$ meV, and $\Delta(L = 1000$ nm$) = 1.41 \times 10^{-7}$ meV.

As the $\lambda_{1,2}$ approaches to constant near $k_x = 0$, $E_{\pm}(k_x) \simeq -MD/B \pm A\sqrt{B_+B_-/B^2}k_x$. For real roots $\lambda_{1,2}$, the function $f_{\pm}(y)$ are distributed dominantly near the edge ($y = \pm L/2$) in the scale of $\lambda_{1,2}^{-1}$. This result is consistent with those by means of the tight binding approximation [9].

In the following we shall concentrate on the real solution of λ with a finite L, i.e. the solutions for the edge states. For real λ and finite L, the right hand side of Eq. (9) is always greater than 2. If $\lambda_{1,2}L >> 1$, it is approximately $2 + 4e^{-2\lambda_2 L}$ (assuming $\lambda_1 >> \lambda_2$). From Eq. (9), it is found that a finite energy gap $\Delta = E_+ - E_-$ opens at $k_x = 0$

$$\Delta \simeq \frac{4|AB_+B_-M|}{\sqrt{B^3(A^2B - 4B_+B_-M)}}e^{-\lambda_2 L}, \quad (12)$$

which decays in an exponential law of L. This is the main consequence in the present work.

In general cases, we have numerical solution of the equations. As a concrete example, we adopt the parameters for the inverted HgTe/CdTe quantum well of thickness $d = 7.0$ nm from the reference [10] for all numerical calculations in the present Letter: $A = 364.5$ meV nm, $B = -686$ meV nm^2, $M = -10$ meV, $D = -512$ meV nm^2. For $L = 1000$ nm, one has $\lambda_1 = 0.7797$ nm^{-1} and $\lambda_2 = 0.0187$ nm^{-1} at $k_x = 0$. The energy gap is very tiny, $\Delta = E_+ - E_- = 1.41 \times 10^{-7}$ meV. However, for $L = 200$ nm at $k_x = 0$, the gap $\Delta = 0.4509$ meV, which becomes large enough to be measurable in experiments. We plot the energy spectra for the edge states of several sizes in Fig. 1(a). However, for a narrow width L (e.g.,

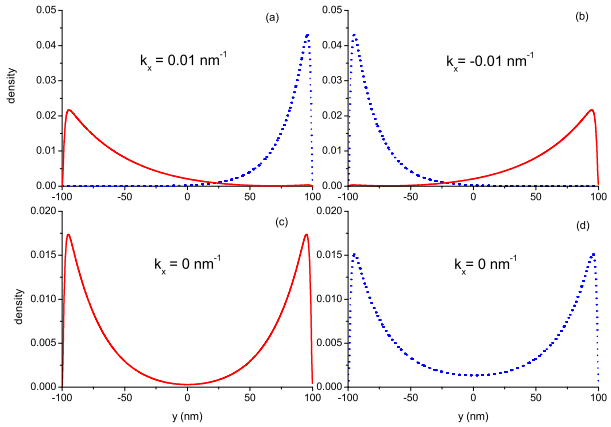

FIG. 2: (Color online) The density distribution of the two edge states $\Psi_{\uparrow\pm}(k_x, y)$ for $L = 200$ nm. (a) The red solid line corresponds to $|\Psi_{\uparrow+}(k_x, y)|^2$ and the blue dotted line to $|\Psi_{\uparrow+}(-k_x, y)|^2$ at $k_x = 0.01$ nm^{-1}; (b) The red solid line corresponds to $|\Psi_{\uparrow-}(k_x, y)|^2$ and the blue dotted line to $|\Psi_{\uparrow-}(-k_x, y)|^2$ at $k_x = -0.01$ nm^{-1}; (c) and (d) for $k_x = 0$ nm^{-1}.

$L = 200$ nm), there is the parabolic-like spectrum near $k_x = 0$. The size-dependence of the energy gap is plotted in Fig. 1(b).

The corresponding wave functions of eigenvalues $E_\pm(k_x)$ yields

$$\Psi_{\uparrow+} = \tilde{c}_+ e^{ik_x x}\left(f_+ + \gamma^+_{k_x} f_-, \eta_1^+ f_- + \gamma^+_{k_x}\eta_2^+ f_+\right)^T, \quad (13)$$

$$\Psi_{\uparrow-} = \tilde{c}_- e^{ik_x x}\left(f_- + \gamma^-_{k_x} f_+, \eta_2^- f_+ + \gamma^-_{k_x}\eta_1^- f_-\right)^T, \quad (14)$$

where

$$\eta_1^\pm = \left.\frac{B_+\left(\lambda_1^2-\lambda_2^2\right)/A}{\lambda_1\coth\frac{\lambda_1 L}{2}-\lambda_2\coth\frac{\lambda_2 L}{2}}\right|_{E=E_\pm},$$

$$\eta_2^\pm = \left.\frac{B_+\left(\lambda_1^2-\lambda_2^2\right)/A}{\lambda_1\tanh\frac{\lambda_1 L}{2}-\lambda_2\tanh\frac{\lambda_2 L}{2}}\right|_{E=E_\pm},$$

$$\gamma^+_{k_x} = \left.\frac{B_+\left(\lambda_1^2-\lambda_2^2\right)k_x\eta_1/\eta_2}{\beta\lambda_1\tanh\frac{\lambda_1 L}{2}-\alpha\lambda_2\tanh\frac{\lambda_2 L}{2}}\right|_{E=E_+},$$

$$\gamma^-_{k_x} = \left.\frac{B_+\left(\lambda_1^2-\lambda_2^2\right)k_x\eta_2/\eta_1}{\beta\lambda_1\coth\frac{\lambda_1 L}{2}-\alpha\lambda_2\coth\frac{\lambda_2 L}{2}}\right|_{E=E_-}.$$

and $\tilde{c}_\pm$ are normalization constants. The solutions can be simplified in the limit of large L as $\eta_1^\pm = \eta_2^\pm = \eta = B_+(\lambda_1+\lambda_2)/A$ and $\gamma^+_{k_x} = -\gamma^-_{k_x} = -\mathrm{sgn}(k_x)$. The other two solutions for the lower block can be produced by means of the time reversal operation, $\Psi_{\downarrow\pm} = \Theta\Psi_{\uparrow\pm}$, and the spectra are degenerate with those of the upper block.

According to the present analytic solutions of wave functions, the density distribution of the functions are mainly determined by the two length scales, $\lambda_{1,2}^{-1}$. In the example in Fig. 1, we notice that $\lambda_2^{-1} >> \lambda_1^{-1}$. For a large size of the sample, the density of the wave function increases in an exponential law in the scale of λ_2^{-1} and then decays exponentially in a scale of λ_1^{-1} near the boundaries, which is consistent with the work by König *et al.*[10] The wave function almost vanishes far away from the boundaries if the width of the sample is much larger than λ_2^{-1}. As an example, the density distributions of $\Psi_{\uparrow\pm}(k_x, y)$ for $L = 200$ nm are plotted for demonstration in Fig. 2 where $\lambda_2^{-1} = 55.9$ nm and 51.8 nm at $k_x = 0$. The states of $\Psi_{\uparrow+}(k_x, y)$ and $\Psi_{\uparrow-}(-k_x, y)$ $(k_x > 0)$ have the same spin $(\propto (1, -\eta)^T$ in the large L limit) and the positive velocity, v_x $(= +A\sqrt{B_+B_-/B^2}) > 0$ when k_x is far away from $k_x = 0$ and the density distribution is located at one side while the states of $\Psi_{\uparrow+}(-k_x, y)$ and $\Psi_{\uparrow-}(+k_x, y)$ $(k_x > 0)$ have another spin $(\propto (1, \eta)^T$ in the large L limit) and a negative velocity, $-v_x < 0$, and are distributed on the other side. From the solution we found that $\Psi_{\uparrow\pm}(k_x, y)$ and $\Psi_{\uparrow\pm}(-k_x, y)$ couple near $k_x = 0$ due to the finite size effect. Consequently, the states with different spins mix together and the densities of the wave functions $\Psi_{\uparrow\pm}(k_x = 0, y)$ are symmetrically distributed at the two sides. This fact is consistent with the opening of an energy gap in the spectra at $k_x = 0$.

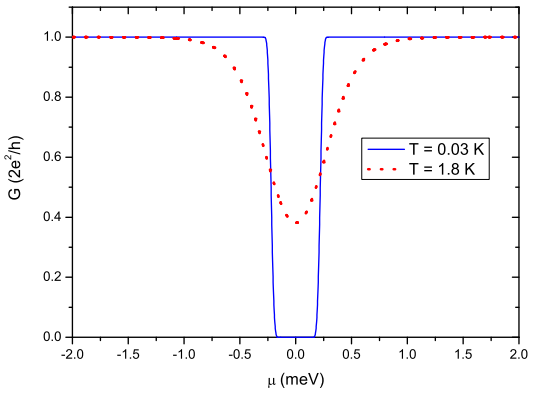

FIG. 3: (Color online) The variations of conductance G via the chemical potential μ inside the bulk insulting gap for a HgTe/CdTe quantum well of $L = 200$ nm at temperatures $T = 30$ mK and 1.8 K, respectively. Note that the energy zero point is shifted to the center of the gap Δ (= 0.4509 meV).

The charge conductance of a QSH phase in a strip was predicted theoretically to be $2e^2/h$ due to the presence of two spin-resolved conducting channels at the edges of the strip, which was observed experimentally in two samples with sizes of (1.0×1.0) μm^2 and (1.0×0.5) μm^2, respectively.[4] The finite size effect will modify the conductance of the QSH phase. Following the Landauer-Büttiker formula,[12] the charge conductance has the form,

$$G(\Delta) = \frac{2e^2}{h}\left[\frac{1}{e^{\left(\frac{\Delta}{2}-\mu\right)/k_BT}+1} - \frac{1}{e^{\left(-\frac{\Delta}{2}-\mu\right)/k_BT}+1} + 1\right].$$

$G(\Delta) \to 2e^2/h$ at low temperatures only when the chemical potential locates out of the gap $\Delta(L)$. Below the temperature of $k_B T^* = \Delta$, a dip will be obviously exhibited. We plot the temperature dependence of the conductance in Fig. 3. In the experiment by König *et al*[4], the smallest sample has $L = 500$ nm, and the measurement was performed at 30 mK. The calculated $\Delta = 1.6 \times 10^{-3}$ meV (19 mK), which is already comparable with the experiment temperature. For a smaller example, the energy gap of $L = 200$ nm is about $\Delta = 0.4509$ meV, and the corresponding temperature is enhanced to $T^* = 5.22$ K. Experimentally, the data for two smaller samples are close to the value of $2e^2/h$ while the data for the wider samples obviously deviate from the value. From the present exact solution, it is believed that the value will be also modified at lower temperatures for even smaller samples. By the way, it is also worth noting that the gap is also highly sensitive to the thickness of quantum well, as all parameters in Eq. (1) are functions of the thickness.

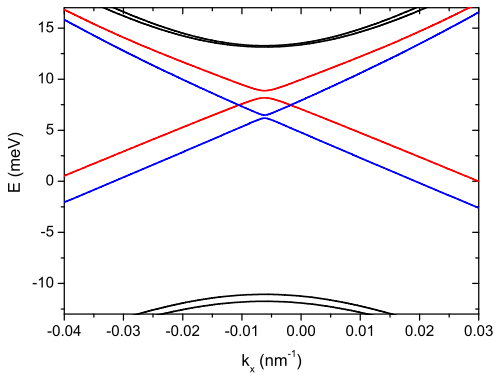

FIG. 4: (Color online) The energy dispersion of the edge states in a weak field of $B = 0.04$T. The blue lines are for the upper block and red lines are for the lower block. The back lines is for the bulk spectra. The width of sample is $L = 200$nm.

Finally, our solution shows that the QSH edge states is quite different from the edge states of a conventional QH strip. For a QH strip with translational symmetry along the strip, the states are classified with the momentum k_x. The edge states at the two sides have different k_x.[13] So they do not mix together even when the two states overlap in the space if there is no other scatterers or interactions in between two edges. In the case of a QSH strip, the edge states at the two sides have the same k_x. Near the anti-crossing points, the two states has the nearly equal energy and momentum. So they can couple together to generate an energy gap when their energies becomes closer and the wave functions have overlaps in a finite space. The magentic field dependence of the QSH edge states also reflects this peculiar property. Consider the sample is subjected to a weak perpendicular magnetic field $\mathbf{B}_z$. Using the Peierls substitution, $k_x \to k_x - eA_x/\hbar$ in Eq.(1) by taking the gauge, $A_x = -B_z y$ (for $|y| < L/2$) and $A_y = 0$ in order to keep k_x a good quantum number. As the wave functions of the edge states decay exponentially, the expectation value of A_x in the two edge states is proportional to L approximately for $L >> \lambda_{1,2}^{-1}$. The energy will be shifted by $\Delta E = +g\mu_B B_z$ ($g \approx m_e v_x \left[L - \lambda_1^{-1} - \lambda_2^{-2} - 2(\lambda_1 + \lambda_2)^{-1}\right]/\hbar$) near $k_x = 0$. Thus the energy spectra of the two edge states of the upper block will shift downward or upward $E(k_x) \approx \pm v_x \hbar k_x + g\mu_B B_z$ for a large L. By increasing the magnetic field B_z the anti-crossing point of energy spectra is eventually moved out of the bulk insulating gap, and the spectra will not crossing in momentum between the gap. However, another two branches of the spectra of the lower block will move in an opposite direction, and the two sets of the spectra may cross in momentum inside the insulating gap. A more detailed calculation is to use the exact solutions of Eqs. (13) and (14) at $B_z = 0$ as a basis to truncate the model of Eq.(1) in a B_z field to an effective one. Numerical results are plotted in Fig.4. The energy shift is very sensitive to the magnetic field and the width of the sample. As for the conductance, the value of $2e^2/h$ will recover near the crossing points. Thus the magnetoresistance is very sensitive to a tiny field, which might have potential application for a sensitive detection.

SQS thanks S. C. Zhang for helpful discussions. This work was supported by the Research Grant Council of Hong Kong under Grant No.: HKU 7042/06P, and the CRCG of the University of Hong Kong.

[1] C. Day, Physics Today **61**, 19 (2008).
[2] C. L. Kane and E. J. Mele, Phys. Rev. Lett. **95**, 146802 (2005); *ibid.* **95**, 226801 (2005).
[3] B. A. Bernevig *et al.*, Science **314**, 1757 (2006).
[4] M. König *et al.*, Science **318**, 766 (2007).
[5] B. A. Bernevig and S. C. Zhang, Phys. Rev. Lett. **96**, 106802 (2006).
[6] S. Murakami, Phys. Rev. Lett. **97**, 236805 (2006);
[7] D. N. Sheng *et al.*, Phys. Rev. Lett. **97**, 036808 (2006); C. Wu, B. A. Bernevig, and S. C. Zhang, *ibid.* **96**, 106401 (2006); M. Onoda *et al.*, *ibid.* **98**, 076802 (2007); C. Xu and J. E. Moore, Phys. Rev. B **73**, 045322 (2006); L. Fu and C. L. Kane, *ibid.* **74**, 195312 (2006); T. Fukui and Y. Hatsugai, *ibid.* **75**, 121403 (2007); H. Obuse *et al.*, *ibid.* **76**, 075301 (2007); S. Murakami, S. Iso, Y. Avishai, M. Onoda, and N. Nagaosa, *ibid.* **76**, 205304 (2007); X. Dai *et al.*, *ibid.* **77**, 125319 (2008); Z. H. Qiao *et al.*, arXiv: 0711.1005.
[8] D. Hsieh *et al.*, Nature 452, 970 (2008).
[9] X. L. Qi *et al.*, Phys. Rev. B **74**, 085308 (2006).
[10] M. König *et al.*, J. Phys. Soc. Jpn 77, 031007 (2008).
[11] A. Pfeuffer-Jeschke, thesis, University of Würzburg (2000).
[12] S. Datta, *Electronic transport in mesoscopic systems*, (Cambridge University Press, Cambridge, 1995).
[13] B. I. Halperin, Phys. Rev. B 25, 2185 (1982); A. H. MacDonald and P. Steda, Phys. Rev. B 29, 1616 (1984).